Biochimica et Biophysica Acta 1842 (2014) 1433–1443

Contents lists available at ScienceDirect

Biochimica et Biophysica Acta

journal homepage: www.elsevier.com/locate/bbadis

Cardiac remodeling associated with protein increase and lipid accumulation in early-stage chronic kidney disease in rats

Mieko Kuwahara [a,b,*], Kenji Bannai [a], Hiroko Segawa [b], Ken-ichi Miyamoto [b], Hideyuki Yamato [a]

[a] Kureha Corporation, Adsorptive Medicine Technology Center, Tokyo, Japan
[b] Department of Molecular Nutrition, Institute of Health Biosciences, University of Tokushima Graduate School, Tokushima, Japan

ARTICLE INFO

Article history:
Received 17 December 2013
Received in revised form 11 April 2014
Accepted 28 April 2014
Available online 2 May 2014

Keyword:
Cardiac remodeling
Chronic kidney disease
FTIR spectroscopy
Uremic toxin
Lipid accumulation

ABSTRACT

Chronic kidney disease (CKD) is associated with increased risks of cardiovascular morbidity and mortality. Cardiac remodeling including myocardial fibrosis and hypertrophy is frequently observed in CKD patients. In this study, we investigate the mechanism involved in cardiac hypertrophy associated with CKD using a rat model, by morphological and chemical component changes of the hypertrophic and non-hypertrophic hearts. Sprague–Dawley rats were 4/5 nephrectomized (Nx) at 11 weeks of age and assigned to no treatment and treatment with AST-120, which was reported to affect the cardiac damage, at 18 weeks of age. At 26 weeks of age, the rats were euthanized under anesthesia, and biochemical tests as well as analysis of cardiac condition were performed by histological and spectrophotometric methods. Cardiac hypertrophy and CKD were observed in 4/5 Nx rats even though vascular calcification and myocardial fibrosis were not detected. The increasing myocardial protein was confirmed in hypertrophic hearts by infrared spectroscopy. The absorption of amide I and other protein bands in hypertrophic hearts increased at the same position as in normal cardiac absorption. Infrared spectra also showed that lipid accumulation was also detected in hypertrophic heart. Conversely, the absorptions of protein were obviously reduced in the myocardium of non-hypertrophic heart with CKD compared to that of hypertrophic heart. The lipid associated absorption was also decreased in non-hypertrophic heart. Our results suggest that cardiac remodeling associated with relatively early-stage CKD may be suppressed by reducing increased myocardial protein and ameliorating cardiac lipid load.

1. Introduction

Patients with chronic kidney disease (CKD) generally have increased risks of complications including accelerated cardiovascular disease compared to the general population [1]. Cardiac mortality is the main cause of death and marked cardiac remodeling is frequently observed in CKD patients [2]. Molecular, cellular and interstitial changes are reported to manifest clinically as changes in size, shape and function of the heart, resulting from cardiac load or injury [3]. Cardiac remodeling is now recognized as an important aspect of cardiovascular disease progression.

Cardiac hypertrophy is the primary mechanism in cardiac remodeling, and is one of the compensatory actions by a large number of physiological and pathological conditions. When hypertrophy occurs, the tension generated by the contraction of the myocardium is increased, and the contractile force of the heart increased. Cardiac hypertrophy has, at the beginning, beneficial effects in terms of muscular economy, normalizing wall stress [4]. However, as hypertrophy progresses, myocardial damage is caused by an imbalance of contraction or excessive stretching. Chronic hypertrophy is reported to be associated with a significant increase in the risk of heart failure, dilated cardiomyopathy, ischemic heart disease, and sudden death, leading to increased cardiovascular mortality [5–9]. Fibrosis is reported to manifest on various morphologically distinct forms [10], and myocardial fibrosis is often observed in hypertrophic heart. In CKD model rats, interstitial fibrosis was reduced by treatment with a calcimimetic, despite no effect on cardiac hypertrophy [11]. Myocardial fibrosis is probably a consequence of hypertrophy. Thus, it is important to prevent the compensated cardiac hypertrophy with CKD, which is the previous stage of decompensated hypertrophy leading to heart failure. Hypertension is often noticed as a cause of cardiac hypertrophy [12]. Inorganic phosphorus (Pi), parathyroid hormone (PTH), fibroblast growth factor 23 (FGF23) and anemia are also regarded recently as candidates associated with cardiac hypertrophy with CKD [13–16]. Various studies have been conducted, but many questions remain unanswered.

It is necessary to confirm the significant changes associated with cardiac pathologies to prevent hypertrophy. Cardiac hypertrophy is more likely to begin at early-stage of renal insufficiency, and only the staining methods have limits to examine the cardiac changes due to

* Corresponding author at: Adsorptive Medicine Technology Center, Kureha Corporation, 3-26-2, Hyakunin-cho, Shinjuku-ku, Tokyo 169-8503, Japan. Tel.: +81 3 3362 7421; fax: +81 3 3362 8522.
E-mail address: kuwahara@kureha.co.jp (M. Kuwahara).

http://dx.doi.org/10.1016/j.bbadis.2014.04.026
0925-4439/

hypertrophy. Spectrophotometric techniques such as Fourier transform infrared (FTIR) spectroscopy have been used for over half a century for structural analysis in biophysics and biochemistry. Recent technological developments in FTIR spectroscopy have enabled the possibility for applications in histopathologic imaging for diagnosis and research of disease. FTIR microspectroscopy provides structural information as well as relative quantification of lipids, proteins, carbohydrates and a variety of phosphorylated biomolecules within biological samples such as cell or tissue [17].

The present study aimed to investigate the mechanism involved in cardiac hypertrophy associated with CKD using a rat model, by morphological and chemical component changes of the hypertrophic heart. In addition, we considered the suppression mechanism of hypertrophy, by using a CKD model rat treated with AST-120 (Kremezin®; Kureha Corporation, Tokyo, Japan) [18,19] that has been reported to prevent the progression of cardiac damage in CKD [20–22].

2. Material and methods

2.1. Surgical model for CKD

Nine-week-old male Sprague–Dawley rats were purchased from Japan SLC, Inc. (Hamamatsu, Japan). At 10 weeks of age (260–280 g in weight), rats were anesthetized with sodium pentobarbital (5 mg/100 g body weight) and the left kidney was resected at top and bottom slant 45° from the center to standardize the size of residual renal tissue in CKD model rats. One week later, right nephrectomy was performed leaving approximately 1/5 of the total renal mass. Six age-matched rats were sham-operated as controls (sham-control group). Seven weeks after nephrectomy, nephrectomized rats were divided into three groups. One group was not treated with AST-120 (non-AST-treated group) and two groups were treated with different doses of AST-120. One AST-120-treated group was fed a diet containing 4% AST-120 (AST-low group) and the other group was fed a diet containing 8% AST-120 (AST-high group). Mean amount of AST-120 dose was calculated from mean food consumption in a day and the result of sample analysis (CE-2 including 25% protein and 5% lipid; CLEA Japan Inc., Tokyo, Japan). Blood samples during experimental period were collected from the jugular vein under anesthesia. At 26 weeks of age, the rats were euthanized under anesthesia after 24-h urine samples were collected using metabolic cages. Blood samples were collected from the abdominal aorta for biochemical measurements, and the hearts and thoracic aortas were removed for weight measurement and the other analyses. All animal care and procedures were approved by the Animal Care and Use Committee of Kureha Corporation.

2.2. Evaluation of cardiac hypertrophy

The weight and cross-sectional area of the heart were measured to evaluate cardiac hypertrophy. Four-μm transverse sections of the heart at the equatorial plane were cut. The section just below the right atrium provides the largest cut surfaces. The cross-sectional areas of hematoxylin and eosin (HE)-stained sections were analyzed using a Leica QwinV3 System (Leica Microsystems, Solms, Germany). Cross-sectional areas of the heart in study groups were expressed as ratios relative to the area in sham-control group.

2.3. Biochemical analysis

After centrifugation, serum and urine samples were stored at 4 °C until analysis. Serum Cr, BUN, total cholesterol (T-Cho), triglycerides (TG) and Pi levels, and urinary Cr and protein levels were measured using a Unicel DxC 600 Clinical System (Beckman Coulter. Inc., CA, USA). Hemoglobin level in blood was measured using a multichannel blood cell counter (XT-2000i; Sysmex Corporation, Hyogo, Japan). Serum levels of PTH, FGF23 and heart-type fatty acid binding protein (H-FABP) and urinary 8-hydroxydeoxyguanosine (8-OHdG) level were measured using enzyme-linked immunosorbent assay kits (PTH: Rat Intact PTH ELISA Kit; Immutopics, CA, USA. FGF23: FGF-23 ELISA Kit; Kainos Laboratories, Tokyo, Japan. H-FABP: Rat H-FABP ELISA Kit; Life Diagnostics, Inc., PA, USA, 8-OHdG: New 8-OHdG Check; Japan Institute for the Control of Aging, Shizuoka, Japan). Serum levels of colon-derived uremic toxins were determined by liquid chromatography with tandem mass spectrometry (LC/ESI-MS/MS) [23].

2.4. Blood pressure measurements

Systolic blood pressure (SBP), diastolic blood pressure (DBP) and heart rate (HR) were measured in conscious, restrained rats by tail-cuff plethysmography (Model BP-98A; Softron, Tokyo, Japan). To reduce the possibility of stress artifacts, the rat was allowed to acclimatize sufficiently and the mean of five measurements was recorded.

2.5. Histological staining

Heart tissues were fixed in 10% formalin, dehydrated at room temperature through an ethanol series and embedded in paraffin. Four-μm serial sections were cut from the paraffin blocks. Sections were stained with HE for routine histology and Masson's trichrome (MT) for interstitial fibrosis.

The HE-stained sections of the thoracic aortas were prepared in the same manner.

2.6. Spectrophotometric analysis

Four-μm sections used in this study were the adjacent sections of the HE-stained sections used for evaluating cross-sectional area of the heart. The sections were mounted on barium fluoride disks for spectrophotometric analysis. FTIR images of a section of the heart were acquired at 25 μm (partial tissue sections) or 50 μm (whole tissue sections) pixel resolution and 8 cm^{-1} spectral resolution with two co-added scans using a Spotlight 400 spectrometer (PerkinElmer, MA, USA). The mean spectrum of each group was composed of the mean spectra of 1500 × 1500 μm area of myocardium in each rat. Background spectra were collected from the same barium fluoride window under identical condition.

Barium fluoride disks of the thoracic aortas were prepared in the same manner. FTIR image of a section of the thoracic aorta was acquired at 6.25 μm pixel resolution and 4 cm^{-1} spectral resolution with two co-added scans.

2.7. Statistical analysis

Data are expressed as means ± SD. One-way analysis of variance followed by Student's t-test (between non-AST-treated and sham-control group) and Tukey–Kramer post-hoc test (among CKD model groups or four groups) was used to compare inter-group differences. Relationships between variables were assessed using univariate linear regression analysis. A P value less than 0.05 was considered statistically significant.

3. Results

3.1. Cardiac hypertrophy in CKD rats

The physical characteristics and biochemical data of the CKD model and sham-control rats at 26 weeks are shown in Table 1. Body weights were similar in two groups. SBP, DBP and HR were significantly elevated in non-AST-treated rats compared to sham-controls. As for kidney function, creatinine clearance (CCr) was significantly lower and serum Cr, BUN and urinary protein were significantly elevated in the groups of non-AST-treated rats (n = 7) compared to sham-control

Table 1
Animal characteristics in chronic kidney disease model and sham-control rats at 26 weeks of age.

	Non-AST-treated (chronic kidney disease, n = 7)	Sham-control (n = 6)
Body weight, g	532.7 ± 24.7	538.9 ± 30.6
Systolic blood pressure, mm Hg	174.5 ± 32.8**	115.5 ± 7.9
Diastolic blood pressure, mm Hg	118.0 ± 19.4**	88.1 ± 4.2
Heart rate, bpm	323.1 ± 26.5**	274.6 ± 15.2
Hemoglobin, g/dL	13.4 ± 0.9**	16.1 ± 0.3
Creatinine clearance (CCr), mL/min	1.28 ± 0.53**	4.48 ± 0.42
Serum creatinine, mg/dL	1.34 ± 0.65**	0.29 ± 0.03
Blood urea nitrogen, mg/dL	72.3 ± 17.5**	20.9 ± 0.6
Urinary protein, mg/day	229.3 ± 118.0**	12.4 ± 3.2
Indoxyl sulfate, mg/dL	0.60 ± 0.24**	0.10 ± 0.03
p-Cresyl sulfate, μg/dL	6.43 ± 3.60**	1.33 ± 0.52
Hippuric acid, mg/dL	0.78 ± 0.33**	0.17 ± 0.06
Inorganic phosphorus, mg/dL	6.26 ± 0.79	5.85 ± 0.34
Parathyroid hormone, pg/mL	2077.7 ± 1942.6	379.2 ± 229.2
Fibroblast growth factor 23, pg/mL	2348.7 ± 2877.7	315.6 ± 43.4
Total cholesterol, mg/dL	119.9 ± 27.8**	47.0 ± 6.4
Triglycerides, mg/dL	254.0 ± 65.2	313.0 ± 77.4
Heart-type fatty acid binding protein, ng/mL	0.87 ± 0.31**	0.25 ± 0.13
8-OHdG (ng/day) corrected by CCr (mL/min)	216.8 ± 136.2**	23.4 ± 10.1

8-OHdG; 8-hydroxydeoxyguanosine, $^{**}P < 0.01$; vs. Sham-control.

group (n = 6). Serum levels of colon-derived uremic toxins [indoxyl sulfate (IS), p-cresyl sulfate (PCS) and hippuric acid (HA)] were elevated significantly in non-AST-treated group compared to sham-control group. Mineral metabolic parameters (serum Pi, PTH and FGF23) did not differ significantly between two groups. In serum lipids and parameter associated with lipid, serum T-Cho and H-FABP levels were significantly elevated in non-AST-treated compared to sham-control group, but serum TG level did not differ between the two groups. Hemoglobin level was significantly lower in non-AST-treated rats compared to sham-controls. Oxidative stress, which was expressed as the CCr-corrected level of urinary 8-OHdG [24], significantly increased in non-AST-treated group compared to sham-control group.

Cardiac hypertrophy was defined as increases in heart weight and ventricular wall thickness. Heart weight was significantly greater in non-AST-treated (1.7-fold vs. sham-control) group compared to sham-control (Fig. 1A). Cross-sectional area of the heart was measured to evaluate the ventricular wall thickness. Cardiac cross-sectional area was significantly greater in non-AST-treated (1.4-fold vs. sham-control) group compared to sham-control group (Fig. 1B).

Fig. 1C shows the HE and MT stained sections of the central portion of the myocardium of representative rats in two groups. In HE-stained sections, the width of myocardial fibers increased clearly in non-AST-treated (heart weight: 1.7-fold vs. sham-control) rats compared to sham-control rat. In MT-stained sections, myocardial fibrosis was not obvious in representative CKD model rat compared to sham-control rat.

3.2. Chemical changes in the hypertrophic heart of CKD model rats

The mean mid-infrared spectra (900–1800 cm^{-1}) of the myocardium in non-AST-treated (CKD rats with hypertrophic heart) and sham-control groups are shown in Fig. 2A. Difference spectrum generated by the subtraction of spectrum of sham-control group from spectrum of non-AST-treated group is shown in Fig. 2B. The absorption of amide I (1651 cm^{-1}) and amide II (1548 cm^{-1}) was obviously increased in the hypertrophic heart. Other protein bands were also confirmed at 1245 (amide III), 1310, 1388 and 1446 cm^{-1}, and these absorptions were increased in hypertrophic hearts. FTIR spectroscopy has been shown to be sensitive to the secondary structure of proteins. The absorption of amide I and other protein bands in hypertrophic hearts were at the same position as in normal cardiac absorption in this study. The FTIR absorbance band centered at 1338 cm^{-1} arises from CH_2 wagging vibration of proline side chains in some collagen types

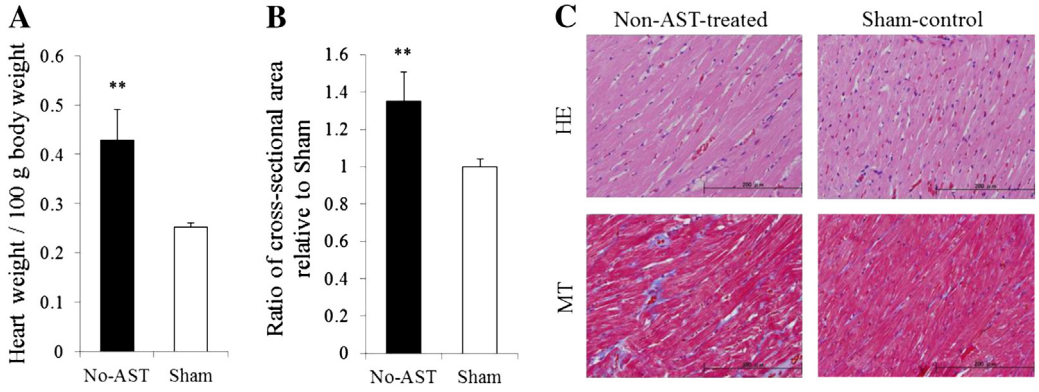

Fig. 1. Cardiac hypertrophy in chronic kidney disease (CKD) model rats. (A) Heart weight in CKD model and sham-operated rats. No-AST, CKD model rats not treated with AST-120 (n = 7); Sham, sham-operated rats (n = 6). Heart weight is expressed as heart weight (g) per 100 g body weight. $^{**}P<0.01$ vs. Sham. (B) Relative cross-sectional area of the heart in CKD model and sham-operated rats. No-AST (n = 7); Sham (n = 6). Relative cross-sectional area is expressed as a ratio relative to that of Sham. $^{**}P<0.01$ vs. Sham. (C) Hematoxylin and eosin staining (HE, upper) and Masson's trichrome staining (MT, lower) (magnification × 40) of the central portion of myocardium in representative rats (non-AST-treated and sham-control groups).

(for example, collagen I, II, III and IV), and it has been utilized to assess the extent of collagen in rat heart [25]. This absorption did not obviously increase in non-AST-treated group compared to sham-control group.

In addition, the 1744 cm^{-1} band arose in hypertrophic hearts. This band is due to the C═O stretching vibration of the ester group in part of the lipids or triglycerides. The molecules forming the cell membrane bilayer are phospholipids. The absorption between 985 and 1140 cm^{-1} are assigned to the v_1, v_3 phosphate vibration [26]. In the difference spectrum (Fig. 2B), the absorption at 1744 cm^{-1} was stronger than the absorption of phosphate vibration.

The total band intensities of each band corrected by cross-sectional area of the heart are shown in Fig. 2C. The total band intensities of phosphate vibration and band associated with collagen did not have significant differences between non-AST-treated and sham-control groups, but the total band intensities of amide I and lipid ester were significantly increased in non-AST-treated group compared to sham-control group.

The FTIR images of amide I (1651 cm^{-1}) and lipid-ester/protein distribution (1744/1651 cm^{-1}) in non-AST-treated and sham-control rats are shown in Fig. 2D. The amide I signal increased in the central portion of the myocardium in non-AST-treated rat, but such increase was not seen in sham-control rat. The lipid-ester/protein signal was stronger in non-AST-treated rat than in sham-control rat.

3.3. Animal characteristics and biochemical measurements among CKD model groups

At 18 weeks of age, body weight, SBP and biochemical data did not differ significantly among CKD model groups (non-AST-treated; n = 7, AST-low group; n = 8, AST-high group; n = 6) (Table 2).

The physical characteristics and biochemical data of CKD model rats at 26 weeks are shown in Table 3. Body weights and food intakes were similar in all groups. Kidney function parameters (CCr, serum Cr, BUN and urinary protein), blood pressure (SBP, DBP and HR), hemoglobin level, mineral metabolic parameters, lipid parameters and oxidative stress had no significant differences among CKD model groups. In serum levels of uremic toxins, PCS and HA did not differ significantly among three groups, but IS was significantly decreased in AST-high group compared to non-AST-treated group.

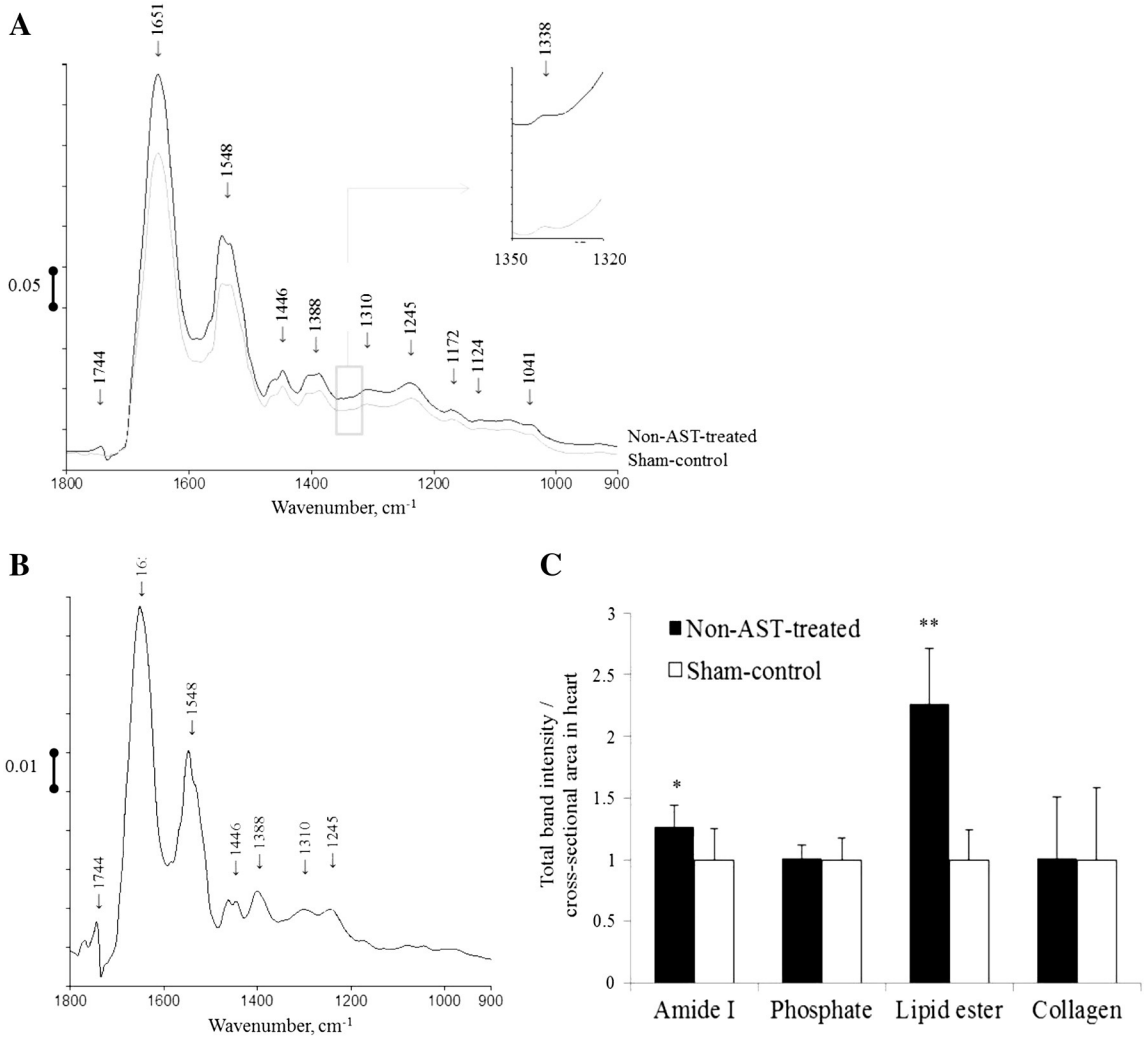

Fig. 2. Fourier transform infrared (FTIR) spectroscopic analyses of hypertrophic heart in chronic kidney disease model rats. (A) Mean mid-infrared spectra of myocardium in non-AST-treated and sham-control groups. Non-AST-treated (n = 7); sham-control (n = 3). (B) Difference spectrum generated by subtraction of sham-control group from non-AST-treated group. Non-AST-treated (n = 7, black line); sham-control (n = 3, gray line). (C) Total band intensities of amide I (1651 cm^{-1}), phosphate (985–1140 cm^{-1}), lipid ester (1744 cm^{-1}) and collagen (1338 cm^{-1}) in hearts. These values are ratio band intensities corrected by the levels of cross-sectional area of the heart. No-AST, Non-AST-treated, n = 7; Sham, sham-control, n = 3. Ratio of band intensity = Total band intensity in each heart divided by the mean total band intensity in sham-control group. $^{**}P < 0.01$, $^{*}P < 0.05$; vs. sham-control. (D) FTIR images of the hearts showing the distribution of amide I (1651 cm^{-1}) and lipid-ester (1744 cm^{-1})/amide I band intensities in representative rats of non-AST-treated (heart weight/body weight; 1.7-fold vs. sham-control) and sham-control groups. The band intensities are depicted in color as illustrated by the adjacent color-bar scale. These representative rats were the same rats used in Fig. 1(C).

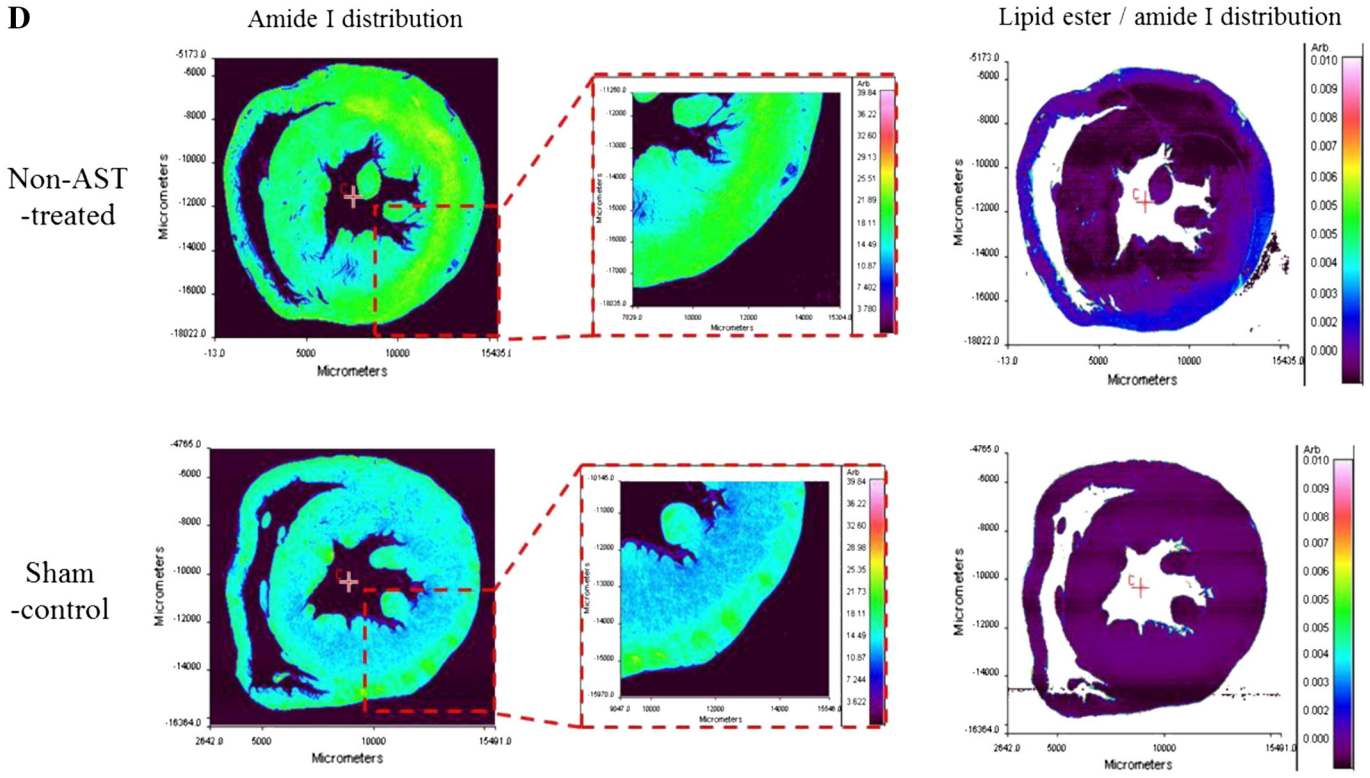

Fig. 2 (*continued*).

Heart weight and cross-sectional area of the heart had no significant differences among CKD model groups (Fig. 3A and B). The doses of AST-120 taken by individual rats at 25–26 weeks varied to some extent in AST-treated groups. The relations between heart weight and AST-120 doses in AST-treated groups are shown in Fig. 3C. A strong negative correlation was observed in AST-low group ($r = -0.805$, $P < 0.05$) as well as in AST-high group ($r = -0.893$, $P < 0.05$).

Cardiac function, which was expressed as rate pressure product (SBP × HR), had a positive correlation with heart weight ($r = 0.773$, $P < 0.01$), but not significantly decreased in AST-treated groups compared to non-AST-treated group (Fig. 3D).

As shown in Table 3, heart weight correlated positively with SBP, DBP, urinary protein, serum levels of Cr, BUN, IS, PCS, HA, Pi, PTH, FGF23, T-Cho, TG, and H-FABP and oxidative stress, and correlated negatively with CCr. Serum levels of Cr, IS, PCS, HA and PTH also had negative correlations with AST-120 doses in both of AST-treated groups.

3.4. Morphologic changes in the myocardium of CKD rats

Fig. 4 shows the HE and MT stained sections of the central portion of the myocardium of representative CKD model rats. The representative rats of the CKD groups had serum Cr levels of approximately 1 mg/dL, and similar body weight, serum Pi and PTH, and SBP levels at 26 weeks of age. In HE-stained sections, the width of myocardial fibers increased approximately 2-fold in non-AST-treated (heart weight: 1.7-fold) and AST-low (heart weight: 1.7-fold vs. sham-control) rats compared to AST-high rat (heart weight: 1.1-fold vs. sham-control). In MT-stained sections, myocardial fibrosis was not obvious in all representative CKD model rats.

3.5. Chemical changes in the heart which is not hypertrophied

The mean mid-infrared spectra in AST-high (CKD model rats without hypertrophic heart, n = 6) and non-AST-treated (CKD model rats with hypertrophic heart, n = 7) groups are shown in Fig. 5A. Difference spectrum generated by the subtraction of spectrum of AST-high group from spectrum of non-AST-treated group is shown in Fig. 5B. AST-120 is an oral charcoal adsorbent, and adsorbs small- and middle-sized hydrophobic molecules in the gastrointestinal tract and is excreted into the feces [27]. Thus, there is not AST-120 in itself to the heart. The absorptions of amide I (1651 cm^{-1}) and amide II (1547 cm^{-1}) were obviously decreased in AST-high group compared to non-AST-treated group.

Table 2
Animal characteristics at 18 weeks of age in chronic kidney disease model rats.

	Non-AST-treated (n = 7)	AST-treated	
		AST-low (n = 8)	AST-high (n = 6)
Body weight, g	473.4 ± 20.2	470.0 ± 31.2	466.5 ± 5.6
Systolic blood pressure, mm Hg	147.8 ± 9.9	145.2 ± 11.6	142.1 ± 4.5
Creatinine clearance, mL/min	1.62 ± 0.16	1.59 ± 0.31	1.78 ± 0.23
Serum creatinine, mg/dL	0.77 ± 0.09	0.80 ± 0.09	0.74 ± 0.11
Blood urea nitrogen, mg/dL	55.9 ± 4.8	59.2 ± 8.1	54.6 ± 5.8
Urinary protein, mg/day	53.5 ± 23.8	64.0 ± 26.2	51.9 ± 20.1
Hemoglobin, g/dL	14.5 ± 0.7	14.6 ± 0.5	14.5 ± 0.6
Total cholesterol, mg/dL	66.9 ± 9.8	72.0 ± 13.2	70.3 ± 11.1
Triglycerides, mg/dL	161.6 ± 40.4	159.4 ± 47.1	145.7 ± 25.4
Inorganic phosphorus, mg/dL	6.49 ± 0.45	6.36 ± 0.44	6.53 ± 0.56

Table 3
Animal characteristics in chronic kidney disease model rats with AST-120 at 26 weeks of age.

	Non-AST-treated (n = 7)	AST-treated		With heart weight/BW	Correlation with AST-120 doses	
		AST-low	AST-high			
		(n = 8)	(n = 6)		AST-low	AST-high
Body weight (BW), g	532.7 ± 24.7	504.9 ± 64.9	495.9 ± 50.4	–	NS	NS
Mean food intake, g/day	21.2 ± 3.0	21.0 ± 4.3	21.5 ± 4.5	NS	–	–
Systolic blood pressure, mm Hg	174.5 ± 32.8	160.2 ± 26.8	162.6 ± 29.2	0.673††	NS	−0.865†
Diastolic blood pressure, mm Hg	118.0 ± 19.4	121.3 ± 23.2	122.6 ± 19.4	0.730††	−0.742†	NS
Heart rate, bpm	323.1 ± 26.5	323.0 ± 14.3	333.6 ± 27.6	NS	NS	NS
Hemoglobin, g/dL	13.4 ± 0.9	13.2 ± 0.7	12.7 ± 1.3	NS	NS	NS
Creatinine clearance (CCr), mL/min	1.28 ± 0.53	1.18 ± 0.67	1.29 ± 1.05	−0.804††	0.723†	NS
Serum creatinine, mg/dL	1.34 ± 0.65	1.45 ± 0.76	1.69 ± 1.22	0.753††	−0.832†	−0.916†
Blood urea nitrogen, mg/dL	72.3 ± 17.5	81.6 ± 32.7	104.9 ± 65.2	0.701††	NS	−0.942††
Urinary protein, mg/day	229.3 ± 118.0	275.1 ± 146.0	231.7 ± 157.4	0.674††	NS	NS
Indoxyl sulfate, mg/dL	0.60 ± 0.24	0.37 ± 0.21	0.23 ± 0.18#	0.530†	−0.724†	−0.967††
p-Cresyl sulfate, μg/dL	6.43 ± 3.60	5.63 ± 5.01	3.33 ± 4.18	0.770††	−0.898††	−0.922††
Hippuric acid, mg/dL	0.78 ± 0.33	0.63 ± 0.33	0.48 ± 0.41	0.754††	−0.749†	−0.957††
Inorganic phosphorus, mg/dL	6.26 ± 0.79	7.16 ± 1.66	7.78 ± 2.31	0.699††	NS	−0.924††
Parathyroid hormone, pg/mL	2077.7 ± 1942.6	2975.3 ± 2823.0	3726.8 ± 3489.3	0.763††	−0.834†	−0.901†
Fibroblast growth factor 23, pg/mL	2348.7 ± 2877.7	27,694.2 ± 71,180.4	34,777.6 ± 68,967.9	0.571††	NS	NS
Total cholesterol, mg/dL	119.9 ± 27.8	151.0 ± 58.8	139.7 ± 67.4	0.810††	−0.780†	NS
Triglycerides, mg/dL	254.0 ± 65.2	306.9 ± 100.4	236.8 ± 110.3	0.524†	NS	−0.860†
Heart-type fatty acid binding protein, ng/mL	0.87 ± 0.31	1.27 ± 1.30	0.70 ± 0.48	0.518†	NS	−0.828†
8-OHdG (ng/day) correlated by CCr (mL/min)	216.8 ± 136.2	174.1 ± 111.8	292.6 ± 277.3	0.565††	NS	−0.958††

NS; not significant difference.
8-OHdG; 8-hydroxydeoxyguanosine, #$P < 0.05$; vs. Non-AST-treated. ††$P < 0.01$, †$P < 0.05$; vs. Heart weight/100 g BW or vs. AST-120 doses.

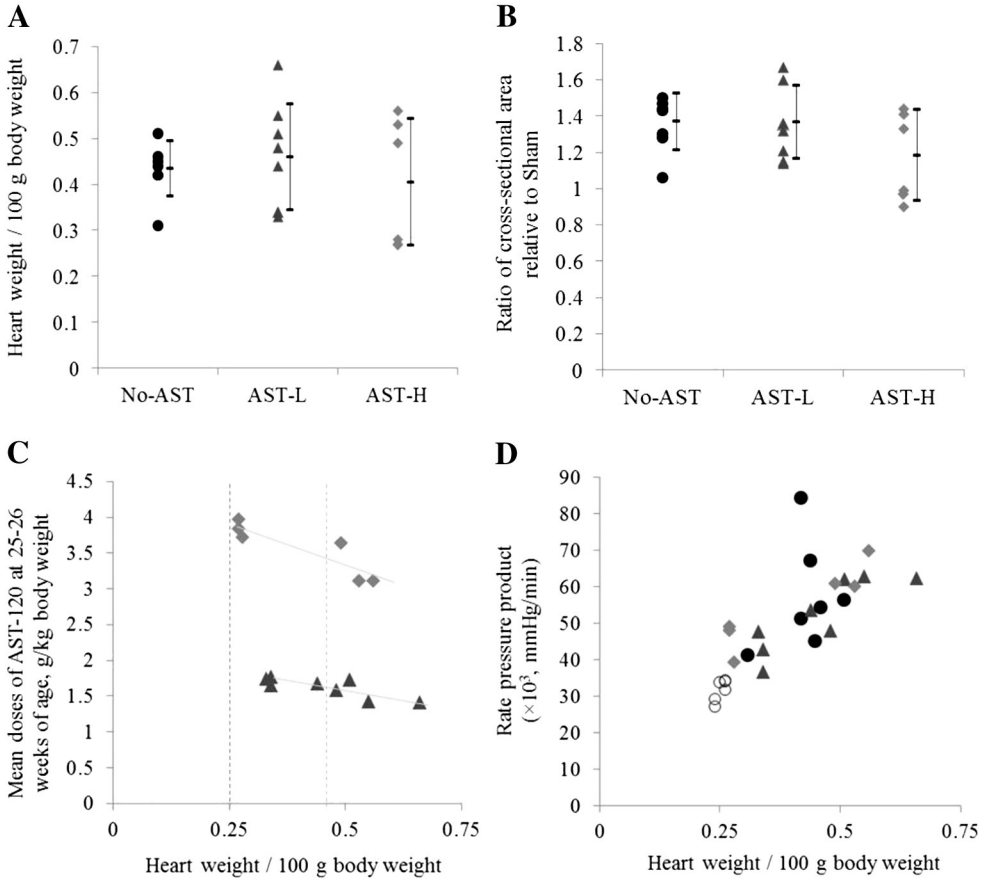

Fig. 3. Cardiac hypertrophy in AST-treated chronic kidney disease (CKD) rats. Heart weight (A) and relative cross-sectional area of the heart (B) in CKD model rats. No-AST (●), non-AST-treated, n = 7; AST-L (▲), AST-low, n = 8; AST-H (◆), AST-high, n = 6. Means ± SD are depicted in the bar next to individual values. (C) Relationship between heart weight and dose of AST-120 at 25–26 weeks in AST-low (▲) and AST-high (◆) groups. AST-low, n = 8; AST-high, n = 6. Correlation between heart weight and dosage of AST-120: at $r = -0.805$, $P < 0.05$ in AST-low group, and $r = -0.893$, $P < 0.05$ in AST-high group. Dark dotted line indicates the mean heart weight of sham-control group, and light dotted line indicates the mean heart weight of non-AST-treated group. (D) Correlation between heart weight and rate pressure product at 26 weeks in non-AST-treated (●), AST-low (▲), AST-high (◆) and sham-control (○) groups ($r = 0.773$, $P < 0.01$). Non-AST-treated, n = 7; AST-low, n = 8; AST-high, n = 6; sham-control, n = 6.

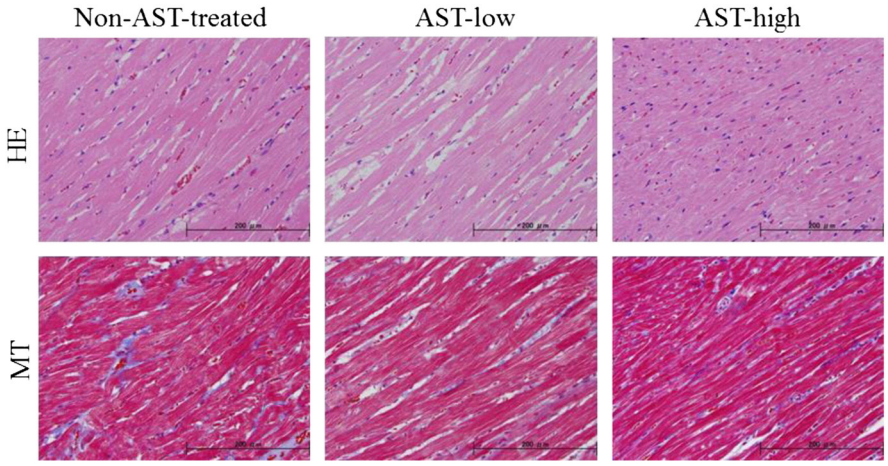

Fig. 4. Hematoxylin and eosin staining (HE, upper) and Masson's trichrome staining (MT, lower) (magnification: ×40) of the central portion of myocardium in representative rats (non-AST-treated, AST-low and AST-high groups).

Other protein bands were also confirmed at 1240, 1312, 1388 and 1447 cm^{-1}, and these absorptions were decreased in non-hypertrophic heart. The absorption at 1744 cm^{-1} was detected in AST-high group, and decreased compared to non-AST-treated group. The absorption of collagen at 1338 cm^{-1} in AST-high group was the same as that in non-AST-treated group. Difference of v_1, v_3 phosphate vibration was not clearly detected between AST-high and non-AST-treated groups.

The total band intensities of each band corrected by cross-sectional area of the heart are shown in Fig. 5C. The total band intensities of amide I, phosphate vibration and the 1338 cm^{-1} band did not have significant differences between AST-high and non-AST-treated groups, but lipid ester was significantly decreased in AST-high group compared to non-AST-treated group.

The FTIR images of amide I (1651 cm^{-1}) and lipid-ester/protein distribution (1744/1651 cm^{-1}) in AST-high rat are shown in Fig. 5D. The increase of amide I signal in the center portion of the myocardium, which was seen in non-AST-treated rat, was not confirmed in AST-high rat. The lipid-ester/protein distribution was weaker in AST-high rat than in non-AST-treated rat.

3.6. The condition of thoracic aortas in CKD model rats

Calcification of thoracic aortas is associated with coronary and valvular calcifications, reflecting an underlying atherosclerotic process [28]. These calcifications have a possibility to associate with increasing cardiac work, promoting heart failure, left ventricular hypertrophy and diastolic dysfunction. Representative mid-infrared spectra of the thoracic aortas in CKD model and sham-control rats are shown in Fig. 6A. There were no obvious differences among four rats. FTIR images of the thoracic aortas had no remarkable differences in phosphate/protein distribution among four rats (Fig. 6B). No definitive differences were detected among all rats by HE staining (data not shown).

3.7. Serum levels of uremic toxins in CKD model and sham-control rats

Uremic toxins are normally excreted by the kidney and interact negatively with biologic functions. A large number of uremic toxins are produced by colon microbes, and may contribute to uremic toxicity [29,30]. AST-120 is known to adsorb these uremic toxins efficiently [31]. The present study showed that serum levels of IS, PCS and HA were decreased in AST-treated groups compared to non-AST-treated group, and have correlation with heart weight and AST-120 doses (Table 3). The dosage of AST-120 was uneven in AST-high group at 7–8 weeks after AST-120 administration (Fig. 7A). During experiment period, serum levels of IS, PCS and HA were decreased significantly in AST-low and AST-high groups compared to non-AST-treated group at 4 weeks after starting AST-120 treatment. However, serum IS level was significantly decreased only in AST-high group and serum levels of PCS and HA were not significantly decreased in AST-treated groups at 8 weeks (Fig. 7B). As shown in Fig. 7C, the heart of AST-high rats, in which levels of serum uremic toxins were similar to those of sham-controls, was not hypertrophied.

4. Discussion

Our study demonstrated the presence of cardiac hypertrophy in 4/5 nephrectomized rats even though myocardial fibrosis was not clearly detected. The infrared spectrum of cardiac and vascular calcification gave absorption peaks corresponding to vibration modes of phosphate [32]. The mid-infrared spectra of heart and thoracic aortas did not have obvious differences in phosphate absorption between CKD model and sham-control rats, suggesting that vascular calcifications were not formed in CKD model rats of this study.

It is the most characteristic in the hypertrophic heart associated with CKD that infrared signal derived from protein was stronger in the central portion of myocardium of hypertrophic heart than that in the same portion of normal heart (Fig. 2). Cardiac remodeling is accompanied by increases in protein synthesis, and wall thickness changes to minimize variability [33,34]. Amide I band of protein has been reported to shift in infarcted heart tissue compared to control tissue [35]. This shift indicated either a structural rearrangement of the existing tissue or the expression of new proteins with different structural characteristics. This study showed that amide I and other protein bands were not seen to shift in CKD model rats compared to sham-control rats, suggesting the amount of the same protein increased in hypertrophic heart tissue. From the results of total band intensity of amide I (Fig. 2C) and distribution (Fig. 2D), the amount of protein per cross-sectional area increased, and proteins increased in the center portion of myocardium before fibrosis was formed. This chronic increase may lead to myocardial fibrosis. In addition, the absorption at 1744 cm^{-1} was stronger than the absorption of phosphate vibration, suggesting that lipids except phospholipid tended to be increased in hypertrophic heart. Ectopic lipid deposition in the heart has been reported in the uninephrectomized rats [36]. Oxidative stress was significantly increased in CKD model rats (Tables 1 and 3), and may lead to the formation of oxidized lipids in cell membranes [37]. The lipid deposition might be lipid peroxide. However, this study was not able to examine it because only lipid ester parts were detected by mid-infrared spectra.

On the other hand, the absorption of band associated with protein was decreased in the myocardium of non-hypertrophic heart compared to hypertrophic heart in CKD model rats. The absorption of lipid ester

was also decreased in non-hypertrophic heart associated with CKD. It is thought to be important for suppression of cardiac hypertrophy in CKD that protein and lipid accumulation are not increased in the myocardium.

The triggers of cardiac hypertrophy induce intercellular signaling cascades that promote protein synthesis and protein stability [33]. The present study showed that serum levels of Cr, PTH and colon-derived uremic toxins (IS, PCS and HA) are associated with cardiac hypertrophy and AST-120 doses. These compounds are classified as uremic toxins [30,38]. A previous study suggests that uremic compounds in blood might reduce inotropy in cultured heart cells and induce arrhythmias, and showed that Cr led to the development of severe arrhythmia joined by impaired contractility [39]. In these parameters, serum levels of IS, PCS and HA may be directly reduced by AST-120 because only these levels were decreased in AST-treated rats compared to non-AST-treated rats. A recent study found that IS may be associated with cardiac remodeling mediated via activation of p38, p42/44 mitogen-activated protein kinase and nuclear factor-kappa B pathways and has pro-fibrotic, pro-hypertrophic and pro-inflammatory effects on cardiac cells [40]. This research suggests that IS may contribute to direct adverse cardiac effects in cell culture at a clinically relevant concentration range. Effects of HA on the heart remain unknown, but in vitro study showed that PCS increases collagen synthesis in cardiac fibrosis and enhances protein synthesis in cardiac myocytes [41]. In this study, Fig. 7B and C suggest a possibility that suppression of hypertrophy in the heart needs reducing the levels of not a specific uremic toxin but various uremic toxins. These data also show the necessity to maintain serum levels of uremic toxins at the same level of normal condition constantly to suppress cardiac hypertrophy with CKD.

Uremic toxins induce the production of reactive oxygen species, which produces oxidative stress, in in vivo studies [42]. Oxidative stress induced by acute ischemia is reported to be involved with the progression of the disease into heart failure, causing fibrosis, left ventricular dysfunction and hypertrophy [37]. The present study showed that oxidative stress was increased in CKD model rats, but decreased in AST-low rats which hearts were hypertrophied compared to

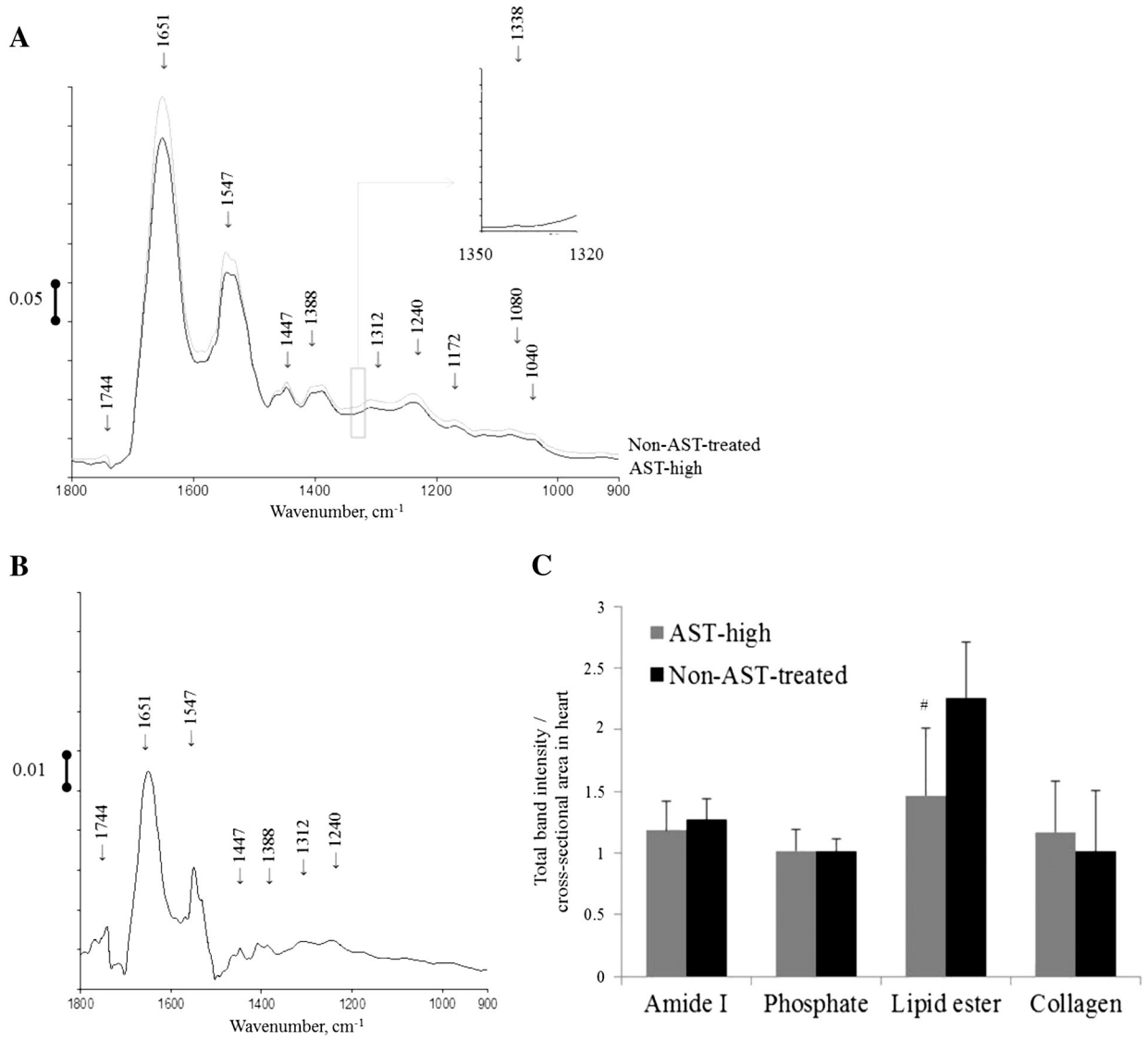

Fig. 5. Fourier transform infrared (FTIR) spectroscopic analyses of non-hypertrophic heart in chronic kidney disease model rats. (A) Mean mid-infrared spectra of myocardium in AST-high and non-AST-treated groups. AST-high (n = 6, black line); non-AST-treated (n = 7, gray line). (B) Difference spectrum generated by subtraction of AST-high group from non-AST-treated group. AST-high (n = 6); non-AST-treated (n = 7). (C) Total band intensities of amide I (1651 cm^{-1}), phosphate (985–1140 cm^{-1}), lipid ester (1744 cm^{-1}) and collagen (1338 cm^{-1}) in hearts. These values are ratio band intensities corrected by the levels of cross-sectional area of the heart. AST-H, AST-high, n = 6; No-AST, non-AST-treated, n = 7. Ratio of band intensity = Total band intensity in each heart divided by the mean total band intensity in sham-control group. $^{\#}P < 0.05$; vs. non-AST-treated. (C) FTIR images of the hearts showing the distribution of amide I (1651 cm^{-1}) and lipid-ester (1744 cm^{-1})/amide I band intensities in representative rats of AST-high [heart weight/body weight (HW/BW); 1.1-fold] and non-AST-treated (HW/BW; 1.7-fold vs. sham-control). The band intensities are depicted in color as illustrated by the adjacent color-bar scale. These representative rats were the same rats used in Fig. 4.

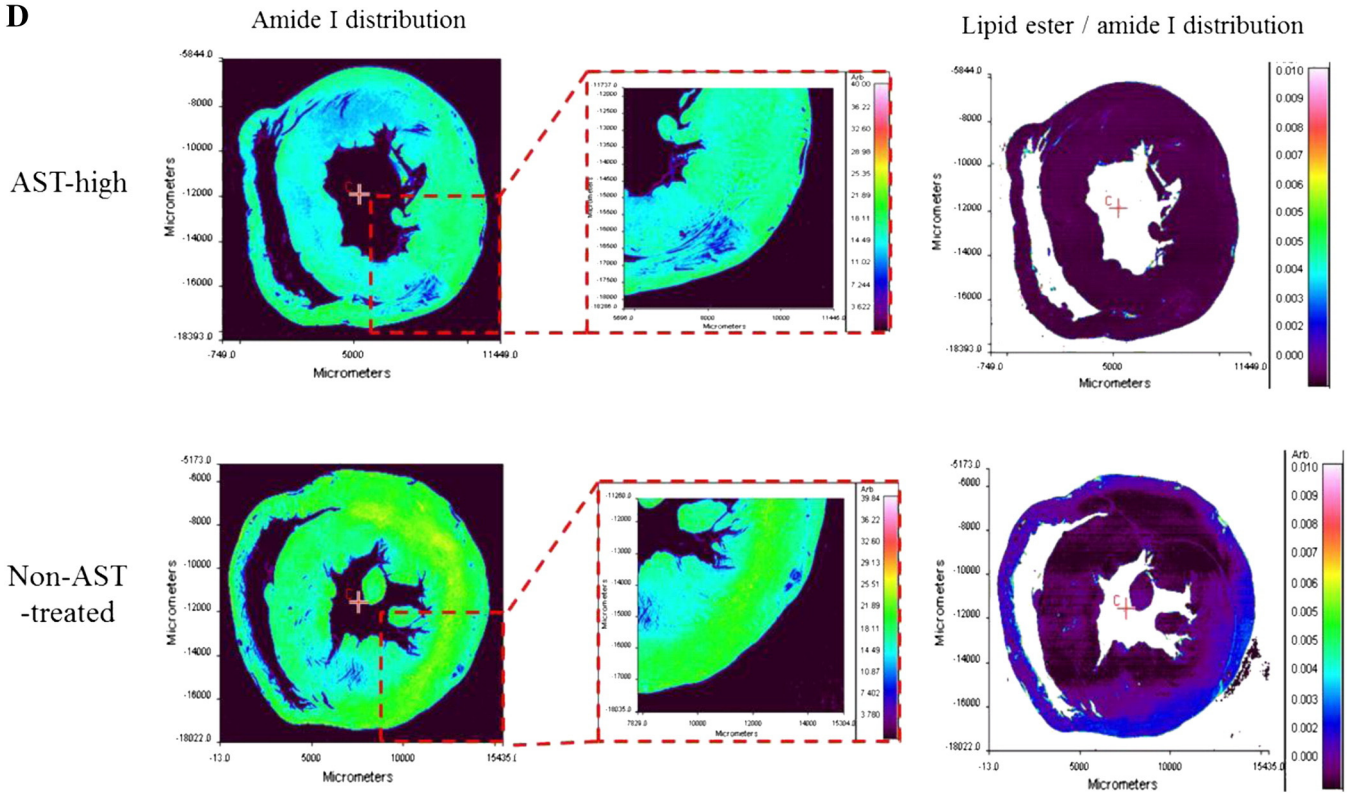

Fig. 5 (*continued*).

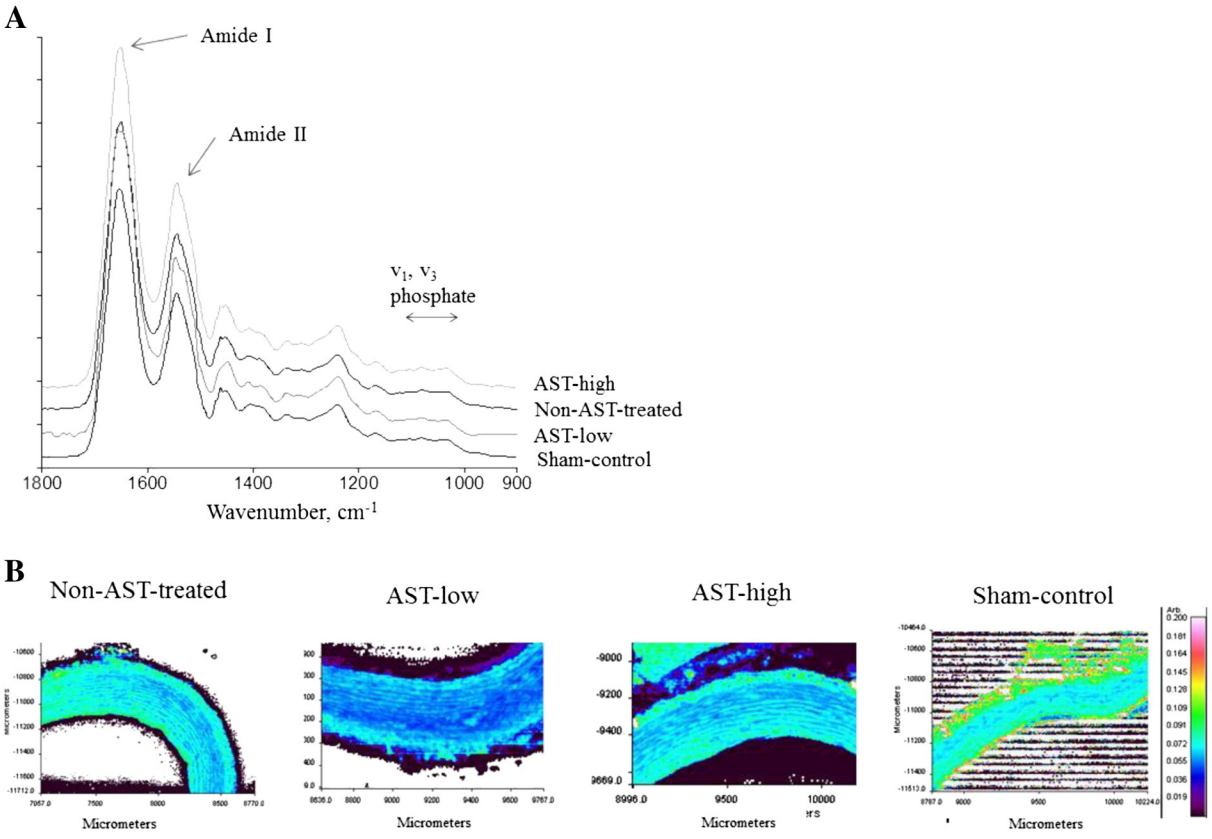

Fig. 6. Spectroscopic analyses of thoracic aortas in representative rats (non-AST-treated, AST-low, AST-high and sham-control groups). These representative rats were the same rats used in Figs. 1(B) and 4. (A) Typical mid-infrared spectra of myocardium in representative rats. Typical peak of phosphate (hydroxyapatite) is at 985–1140 cm^{-1}. (B) Portions of FTIR images of thoracic aortas showing the distribution of phosphate/amide I (1650 cm^{-1}) band intensities in representative rats.

non-AST-treated and AST-high rats (Table 3). Oxidative stress induced by uremic toxins may play an important role in the development of cardiac abnormality, but hypertrophy is not induced only by oxidative stress.

Several studies suggest that a forced reduction in cardiac utilization of fatty acids may trigger the cardiac hypertrophic problem [43]. The H-FABP is involved in fatty acid metabolism by directly mediating transport of long-chain fatty acids in cardiomyocytes, and is released into the bloodstream after myocardial damage [44]. In this study, serum H-FABP level was significantly increased in CKD, but did not have significant differences among CKD model rats, suggesting that myocardial lipid accumulation may not be a major factor associated with hypertrophy in this condition. Previous study proposed that lipid accumulation in failing myocardium has a possibility to increase the levels of toxic intermediates leading to lipotoxicity and the amount and composition of lipids in the myocardium contributes to the development of cardiac dysfunction [45]. It is surely important that the lipid load in the myocardium is reduced to ameliorate cardiac abnormalities.

In conclusion, the present study found that the increase of protein and lipid in myocardium was associated with cardiac remodeling in CKD model rats. It suggests a possibility that high serum levels of some uremic toxins and lipid accumulation in myocardium might be involved in mechanisms of cardiac remodeling at the stage of moderate renal dysfunction before vascular calcification and myocardial fibrosis are established. Cardiac remodeling is essentially a protective

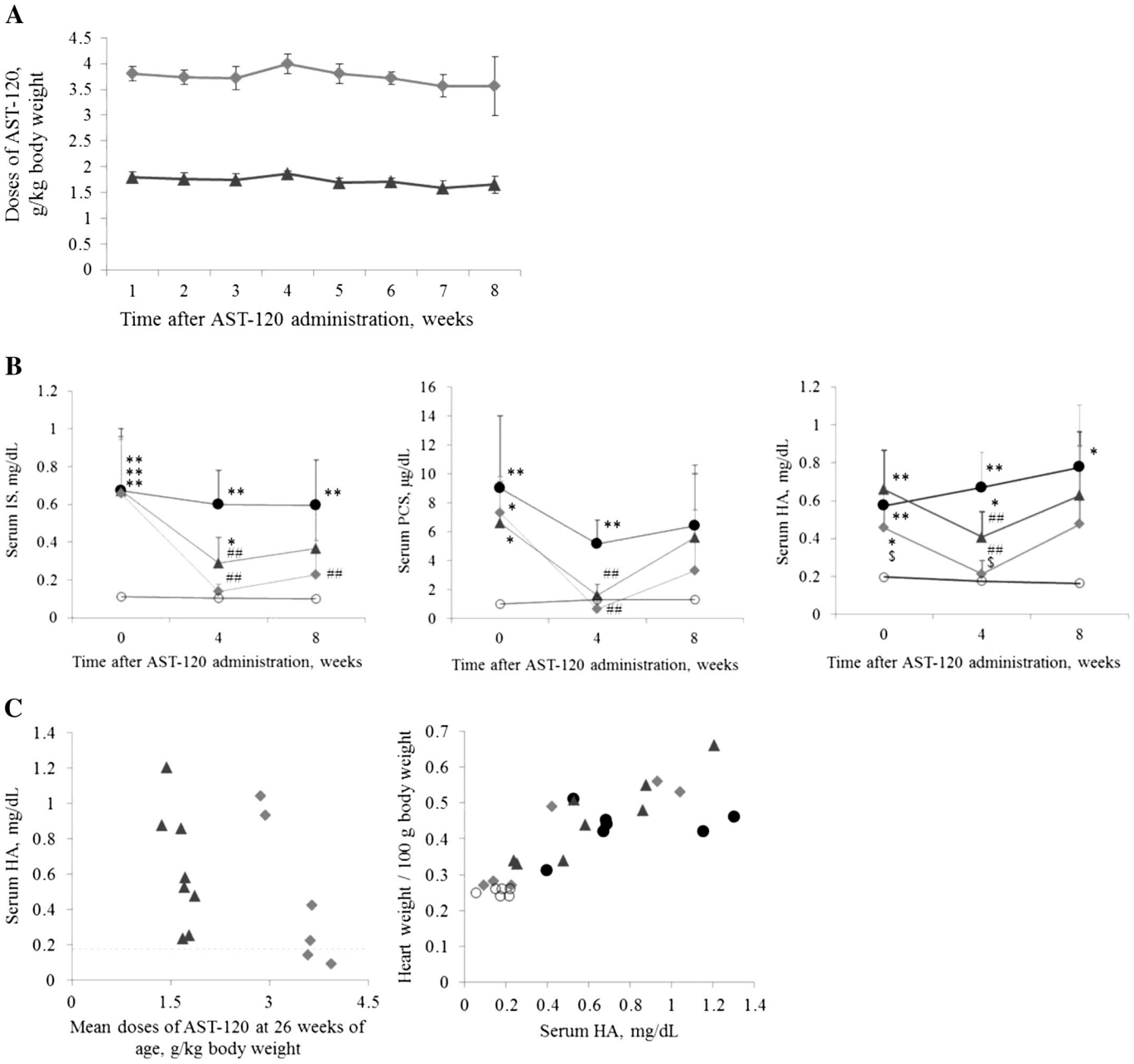

Fig. 7. Serum levels of colon-derived uremic toxins in non-AST-treated (●, n = 7), AST-low (▲, n = 8), AST-high (◆, n = 6) and sham-control (○, n = 6) rats. (A) Changes in doses of AST-120 in AST-treated rats. (B) Changes in serum levels of indoxyl sulfate (IS, left), p-cresyl sulfate (PCS, middle) and hippuric acid (HA, right). $^{**}P < 0.01$, $^{*}P < 0.05$; vs sham-control. $^{\#\#}P < 0.01$; vs non-AST-treated. $^{\$}P < 0.05$; vs AST-low. (C) Correlation between AST-120 doses and serum levels of HA (left). Dotted line indicates the mean serum HA level of sham-control group. Correlation between heart weight and serum levels of HA (right, $r = 0.829$, $P < 0.01$).

mechanism. The indirect control is necessary for the management of cardiac remodeling associated with CKD.

Conflict of interest statement

The authors declare that there is no conflict of interest.

Acknowledgement

The authors are grateful to Hisamitsu Tanaka for advice on cardiac pathology, and Akihiro Ohnishi and Hiromi Kimura-Suda for technical support in FTIR analysis. We thank Kaori Kikuchi for assistance with LC/ESI-MS/MS analysis. We also thank members of Adsorptive medicine and pharmacology section of Kureha Corporation for technical assistance with animal surgery.

References

[1] A.S. Go, G.M. Chertow, D. Fan, C.E. McCulloch, C. Hsu, Chronic kidney disease and the risks of death, cardiovascular events, and hospitalization, N. Engl. J. Med. 351 (2004) 1296–1305.
[2] R.J. Glassock, R. Pecoits-Filho, S.H. Barberato, Left ventricular mass in chronic kidney disease and ESRD, Clin. J. Am. Soc. Nephrol. 4 (2009) S79–S91.
[3] J.N. Cohn, R. Ferrari, N. Sharpe, on behalf of an International Forum on Cardiac Remodeling, Cardiac remodeling—concepts and clinical implications: a consensus paper from an international forum on cardiac remodeling, J. Am. Coll. Cardiol. 35 (2000) 569–582.
[4] M.A. James, A.M. Saadeh, J.V. Jones, Wall stress and hypertension, J. Cardiovasc. Risk 7 (2000) 187–190.
[5] D. Levy, R.J. Garrison, D.D. Savage, W.B. Kannel, W.P. Castelli, Prognostic implications of echocardiographically determined left ventricular mass in the Framingham heart study, N. Engl. J. Med. 322 (1990) 1561–1566.
[6] P.N. Casale, R.B. Devereux, M. Milner, G. Zullo, G.A. Harshfield, T.G. Pickering, J.H. Laragh, Value of echocardiographic measurement of left ventricular mass in predicting cardiovascular morbid events in hypertensive men, Ann. Intern. Med. 105 (1986) 173–178.
[7] M.J. Koren, R.B. Devereux, P.N. Casale, D.D. Savage, J.H. Laragh, Relation of left ventricular mass and geometry to morbidity and mortality in uncomplicated essential hypertension, Ann. Intern. Med. 114 (1991) 345–352.
[8] B.A. Vakili, P.M. Okin, R.B. Devereux, Prognostic implications of left ventricular hypertrophy, Am. Heart J. 141 (2001) 334–341.
[9] L. Bolognese, P. Dellavesa, L. Rossi, G. Sarasso, A.S. Bongo, M. Scianaro, Prognostic value of left ventricular mass in uncomplicated acute myocardial infarction and one-vessel coronary artery disease, Am. J. Cardiol. 73 (1994) 1–5.
[10] K.T. Weber, Extracellular matrix remodeling in heart failure: a role for de novo angiotensin II generation, Circulation 96 (1997) 4065–4082.
[11] N. Koleganova, G. Piecha, E. Ritz, R. Bekeredjian, P. Schirmacher, C.P. Schmitt, M.L. Gross, Interstitial fibrosis and microvascular disease of the heart in uremia: amelioration by a calcimimetic, Lab. Invest. 89 (2009) 520–530.
[12] V. Raizada, D. Hillerson, J.S. Amaram, B. Skipper, Angiotensin II-mediated left ventricular abnormalities in chronic kidney disease, J. Investig. Med. 60 (2012) 785–791.
[13] C.D. Chue, N.C. Edwards, W.E. Moody, R.P. Steeds, J.N. Townend, C.J. Ferro, Serum phosphate is associated with left ventricular mass in patients with chronic kidney disease: a cardiac magnetic resonance study, Heart 98 (2012) 219–224.
[14] M.R. Custodio, M.K. Koike, K.R. Neves, L.M. dos Reis, F.G. Graciolli, C.L. Neves, D.G. Batista, A.O. Magalhaes, P. Hawlitschek, I.B. Oliveira, W.V. Dominguez, R.M.A. Moyses, V. Jorgetti, Parathyroid hormone and phosphorus overload in uremia: impact on cardiovascular system, Nephrol. Dial. Transplant. 27 (2012) 1437–1445.
[15] C. Faul, A.P. Amaral, B. Oskouei, M.C. Hu, A. Sloan, T. Isakova, O.M. Gutierrez, R. Aguillon-Prada, J. Lincoln, J.M. Hare, P. Mundel, A. Morales, J. Scialla, M. Fischer, E. Z. Soliman, J. Chen, A.S. Go, S.E. Rosas, L. Nessel, R.R. Townsend, H.I. Feldman, M.S. J. Sutton, A. Ojo, C. Gadegbeku, G.S.D. Marco, S. Reuter, D. Kentrup, K. Tiemann, M. Brand, J.A. Hill, O.W. Moe, M. Kuro-o, J.W. Kusek, M.G. Keane, M. Wolf, FGF23 induces left ventricular hypertrophy, J. Clin. Invest. 121 (2011) 4393–4408.
[16] M. Suzuki, Y. Hada, M. Akaishi, M. Hiroe, K. Aonuma, Y. Tsubakihara, T. Akizawa, Effects of anemia correction by erythropoiesis-stimulating agents on cardiovascular function in non-dialysis patients with chronic kidney disease, Int. Heart J. 53 (2012) 238–243.
[17] N. Toyran, P. Lasch, D. Naumann, B. Turan, F. Severcan, Early alterations in myocardia and vessels of the diabetic rat heart: an FTIR microspectroscopic study, Biochem. J. 397 (2006) 427–436.
[18] T. Shoji, A. Wada, K. Inoue, D. Hayashi, K. Tomida, Y. Furumatsu, T. Kaneko, N. Okada, Y. Fukuhara, E. Imai, Y. Tsubakihara, Prospective randomized study evaluating the efficacy of the spherical adsorptive carbon AST-120 in chronic kidney disease patients with moderate decrease in renal function, Nephron Clin. Pract. 105 (2007) c99–c107.
[19] T. Akizawa, Y. Asano, S. Morita, T. Wakita, Y. Onishi, S. Fukuhara, F. Gejyo, S. Matsuo, N. Yorioka, K. Kurokawa, on behalf of the CAP-KD Study Group, Effect of a carbonaceous oral adsorbent on the progression of CKD: a multicenter, randomized, controlled trial, Am. J. Kidney Dis. 54 (2009) 459–467.
[20] H. Fujii, F. Nishijima, S. Goto, M. Sugano, H. Yamato, R. Kitazawa, S. Kitazawa, M. Fukagawa, Oral charcoal adsorbent (AST-120) prevents progression of cardiac damage in chronic kidney disease through suppression of oxidative stress, Nephrol. Dial. Transplant. 24 (2009) 2089–2095.
[21] K. Nakai, H. Fujii, K. Kono, S. Goto, M. Fukagawa, S. Nishi, Effects of AST-120 on left ventricular mass in predialysis patients, Am. J. Nephrol. 33 (2011) 218–223.
[22] S. Goto, K. Kitamura, K. Kono, K. Nakai, H. Fujii, S. Nishi, Association between AST-120 and abdominal aortic calcification in predialysis patients with chronic kidney disease, Clin. Exp. Nephrol. 17 (2013) 365–371.
[23] K. Kikuchi, Y. Itoh, R. Tateoka, A. Ezawa, K. Murakami, T. Niwa, Metabolomic search for uremic toxins as indicators of the effect of an oral sorbent AST-120 by liquid chromatography/tandem mass spectrometry, J. Chromatogr. B Analyt. Technol. Biomed. Life Sci. 878 (2010) 2997–3002.
[24] H. Kasai, H. Hayami, Z. Yamaizumi, H. Saito, S. Nishimura, Detection and identification of mutagens and carcinogens as their adducts with guanosine derivatives, Nucleic Acids Res. 12 (1984) 2127–2136.
[25] R. Cheheltani, J.M. Rosano, B. Wang, A.K. Sabri, N. Pleshko, M.F. Kiani, Fourier transform infrared spectroscopic imaging of cardiac tissue to detect collagen deposition after myocardial infarction, J. Biomed. Opt. 17 (2012) 056014.
[26] A.L. Boskey, R. Mendelsohn, Infrared spectroscopic characterization of mineralized tissues, Vib. Spectrosc. 38 (2005) 107–114.
[27] T. Niwa, T. Yazawa, M. Ise, M. Sugano, T. Kodama, Y. Uehara, K. Maeda, Inhibitory effect of oral sorbent on accumulation of albumin-bound indoxyl-sulfate in serum of experimental uremic rats, Nephron 57 (1991) 84–88.
[28] A. Eisen, A. Tenenbaum, N. Koren-Morag, D. Tanne, J. Shemesh, M. Imazio, E.Z. Fisman, M. Motro, E. Schwammenthal, Y. Adler, Calcification of the thoracic aorta as detected by spiral computed tomography among stable angina pectoris patients; association with cardiovascular events and death, Circulation 118 (2008) 1328–1334.
[29] P. Evenepoel, B.K.I. Meijers, B.R.M. Bammens, K. Verbeke, Uremic toxins originating from colonic microbial metabolism, Kidney Int. Suppl. 76 (2009) S12–S19.
[30] E. Schepers, G. Glorieux, R. Vanholder, The gut: the forgotten organ in uremia? Blood Purif. 29 (2010) 130–136.
[31] S. Goto, K. Yoshiya, T. Kita, H. Fujii, N. Fukagawa, Uremic toxins and oral adsorbents, Ther. Apher. Dial. 15 (2011) 132–134.
[32] S.R. Contiguglia, A.C. Alfrey, N.L. Miller, D.E. Runnells, R.Z. Le Geros, Nature of soft tissue calcification in uremia, Kidney Int. 4 (1973) 229–235.
[33] J.A. Hill, E.N. Olson, Cardiac plasticity, N. Engl. J. Med. 358 (2008) 1370–1380.
[34] J.V. Jones, A.S. Serafi, M.A. James, Wall stress and the heart, J. Cardiovasc. Risk 7 (2000) 159–161.
[35] K.Z. Liu, M. Jackson, M.G. Sowa, H. Ju, I.M.C. Dixon, H.H. Mantsch, Modification of the extracellular matrix following myocardial infarction monitored by FTIR spectroscopy, Biochim. Biophys. Acta 1315 (1996) 73–77.
[36] H.L. Zhao, Y. Sui, L. He, J. Guan, S.J. Xiao, D.R. Zhong, Q. Xu, S.E. Zeng, Lipid partitioning after uninephrectomy, Acta Diabetol. 48 (2011) 317–328.
[37] R. Ferrari, L. Agnoletti, L. Comini, G. Gaia, T. Bachetti, A. Cargnoni, C. Ceconi, S. Curello, O. Visioli, Oxidative stress during myocardial ischaemia and heart failure, Eur. Heart J. 19 (1998) B2–B11.
[38] R. Vanholder, R. De Smet, G. Glorieux, A. Argiles, U. Baurmeister, P. Brunet, W. Clark, G. Cohen, P.P. De Deyn, R. Deppisch, B. Descamps-Latscha, T. Henle, A. Jorres, H.D. Lemke, Z.A. Massy, J. Passlick-Deetjen, M. Rodriguez, B. Stegmayr, P. Stenvinkel, C. Tetta, C. Wanner, W. Zidek, European Uremic Toxin Work Group (EUTox), Review on uremic toxins: classification, concentration, and interindividual variability, Kidney Int. 63 (2003) 1934–1943.
[39] D. Weisensee, I. Low-Friedrich, M. Riehle, J. Bereiter-Hahn, W. Schoeppe, In vitro approach to 'uremic cardiomyopathy', Nephron 65 (1993) 392–400.
[40] S. Lekawanvijit, A. Adrahtas, D.J. Kelly, A.R. Kompa, B.H. Wang, H. Krum, Does indoxyl sulfate, a uraemic toxin, have direct effects on cardiac fibroblasts and myocytes? Eur. Heart J. 31 (2010) 1771–1779.
[41] S. Lekawanvijit, A.R. Kompa, B.H. Wang, D.J. Kelly, H. Krum, Cardiorenal syndrome: the emerging role of protein-bound uremic toxins, Circ. Res. 111 (2012) 1470–1483.
[42] L. Dou, N. Jourde-Chiche, V. Faure, C. Cerini, Y. Berland, F. Dignat-George, P. Brunet, The uremic solute indoxyl sulfate induces oxidative stress in endothelial cells, J. Thromb. Haemost. 5 (2007) 1302–1308.
[43] P.M. Barger, D.P. Kelly, Fatty acid utilization in the hypertrophied and failing heart: molecular regulatory mechanisms, Am. J. Med. Sci. 318 (1999) 36–42.
[44] B. Binas, H. Danneberg, J. McWhir, L. Mullins, A.J. Clark, Requirement for the heart-type fatty acid binding protein in cardiac fatty acid utilization, FASEB J. 13 (1999) 805–821.
[45] P.C. Schulze, Myocardial lipid accumulation and lipotoxicity in heart failure, J. Lipid Res. 50 (2009) 2314–2323.